Nationaal Lucht- en Ruimtevaartlaboratorium
National Aerospace Laboratory NLR

NLR-TP-2001-135

Location of rotating sources by phased array measurements

P. Sijtsma, S. Oerlemans and H. Holthusen*

* German Dutch Wind Tunnels DNW-LLF

This report is based on a presentation held at the 7th AIAA/CEAS Aeroacoustics Conference, Maastricht, The Netherlands, 28-30 May 2001.

Division:	Fluid Dynamics
Issued:	26 March 2001
Classification of title:	Unclassified

Contents

16 Figures

(13 pages in total)

AIAA 2001-2167

LOCATION OF ROTATING SOURCES BY PHASED ARRAY MEASUREMENTS

Pieter Sijtsma*, Stefan Oerlemans†
National Aerospace Laboratory NLR, 8300 AD Emmeloord, The Netherlands
and
Hermann Holthusen‡
German Dutch Wind Tunnels DNW-LLF, 8300 AD Emmeloord, The Netherlands

A method is described for the location of moving sources by a microphone array. This method can be applied to out-of-flow measurements in an open jet wind tunnel. For that purpose, an expression is derived for the pressure field of a moving monopole in a uniform flow. It is argued that the open jet shear layer does not form a serious obstacle. A technique is described for reconstruction of power spectra with high signal/noise ratio. The method was implemented for rotating sources, resulting in the computer program ROSI ("ROtating Source Identifier"). Applications of ROSI are given for rotating whistles, blades of a helicopter in hover and wind turbine blades. The test with the rotating whistles demonstrated convincingly the capability to reconstruct the emitted sound. On the helicopter blades, rotating broadband noise sources were made clearly visible. On the wind turbine blades, noise emitted from the leading and trailing edge could be distinguished well.

Nomenclature

$\vec{e}_x$ = unit vector in *x*-direction
G = Green's function, Eq. (6)
M = Mach number of uniform flow
N = number of microphones
p = acoustic pressure
Q = inner product, Eq. (11)
T = transfer function, Eq. (12)
$\vec{x}$ = receiver position
$\vec{x}_n$ = microphone position
δ = Dirac delta function
$\varepsilon_n(t)$ = noise, Eq. (14)
$\chi_n(t)$ = microphone signal
$\sigma(t)$ = source signal
$\tilde{\sigma}(t)$ = reconstructed source signal
$\tilde{\sigma}_n(t)$ = partly reconstructed source signal, Eq. (20)
τ_e = emission time
$\vec{\xi}(t)$ = source position
D/Dt = convective derivative ($= \partial/\partial t + M\,\partial/\partial x$)
$\Im$ = Fourier transform

*Research Engineer, Aeroacoustics Department, P.O. Box 153, e-mail: sijtsma@nlr.nl.
†Research Engineer, Aeroacoustics Department, P.O. Box 153, e-mail: stefan@nlr.nl.
‡P.O. Box 175, e-mail: holthuse@nlr.nl.

I. Introduction

In the last decade, microphone arrays have become more and more in use as a standard tool for acoustic source location. The increasing capacity of computers and data acquisition systems have enabled the use of large numbers of microphones, long acquisition times and high sample frequencies[1]. Thus, the traditional drawbacks of microphone arrays compared to acoustic mirrors, namely lower resolution and lower signal/noise ratio, are vanishing. What remains is the great advantage of arrays, that is, the short time needed for measurements.

In addition, microphone arrays offer the opportunity to locate sources on moving objects. This application, which is relatively new, has been implemented on trains passing by[2,3] and on aeroplanes flying over[4,5]. Source signals in the moving frame were recalculated from the microphone signals, using the technique of de-Dopplerisation[6,7].

The above mentioned examples of array measurements apply to objects in steady, rectilinear motion. There is, however, no need for a restriction to such a motion. In this paper, it is shown that acoustic source location by a microphone array is, in principle, possible on objects in any subsonic motion. Besides,

it is made clear that the presence of a uniform flow does not form any limitation. Therefore, source location measurements on arbitrarily moving objects in wind tunnels are feasible too. Moreover, after some modification, the technique can also be applied to out-of-flow array measurements.

For array measurements on moving objects, the correct acoustic transfer function from moving source to receiver is required, incorporating the effect of Doppler frequency shift. For that purpose, an expression is used for a moving monopole source in a uniform flow. A brief derivation of such an expression is given in this paper. For a more thorough approach, the reader is referred to Howe[8].

Using this transfer function, and by proper interpolation of the sampled microphone data, the emitted signals can be reconstructed. This is necessarily a time-domain technique. It will be explained, however, that the signal/noise ratio can be enlarged by a technique, which is similar to the frequency-domain technique of removing the main diagonal in the cross-correlation matrix.

The technique of acoustic signal reconstruction of moving sources was applied to a special type of motion: rotation. A computer program, named ROSI ("ROtating Source Identifier"), was written to locate rotating sources in a uniform flow, using microphone array measurements. The motivation to develop ROSI was to have the ability to locate and estimate trailing edge noise sources on blades of a wind turbine model in the open jet of the DNW-LLF using an out-of-flow acoustic array[9].

This application, which turned out to be successful, was preceded by two other experiments. First, a test was conducted with rotating whistles, producing tonal noise, in the anechoic chamber of the NLR Small Anechoic Wind Tunnel KAT. This set-up was designed specifically to test the software. Secondly, measurements were carried out on helicopter blades in the open jet of the DNW-LLF.

In this paper, the theory behind ROSI is described and typical results of the three experiments are given.

II. Theory

General

In the analysis that follows, a Cartesian coordinate system (x, y, z) is used, with the x-axis in the direction of the flow. All physical quantities are made dimensionless. The main flow is assumed to be uniform, having Mach number M.

Moving monopole in uniform flow

The acoustic pressure field p of a monopole source moving in a uniform flow is governed by the differential equation

$$\nabla^2 p - \frac{D^2 p}{Dt^2} = \sigma(t)\delta\left(\vec{x} - \vec{\xi}(t)\right), \tag{1}$$

in which $\sigma(t)$ is the source signal emitted by the monopole and $\vec{\xi}(t)$ its time-dependent position. The "convective derivative" D/Dt is defined by

$$\frac{D}{Dt} = \frac{\partial}{\partial t} + M\frac{\partial}{\partial x}. \tag{2}$$

Following Dowling and Ffowcs Williams[10], Eq. (1) can be solved by writing the right-hand side as a superposition:

$$\nabla^2 p - \frac{D^2 p}{Dt^2} = \int_{-\infty}^{\infty} \sigma(\tau)\delta\left(\vec{x} - \vec{\xi}(\tau)\right)\delta(t-\tau)d\tau\,. \tag{3}$$

Then, the solution can be expressed as

$$p(\vec{x}, t) = \int_{-\infty}^{\infty} \sigma(\tau) G\left(\vec{x}, \vec{\xi}(\tau), t, \tau\right) d\tau\,, \tag{4}$$

where G is a solution of

$$\nabla^2 G - \frac{D^2 G}{Dt^2} = \delta\left(\vec{x} - \vec{\xi}(\tau)\right)\delta(t-\tau)\,. \tag{5}$$

The causal solution of Eq. (5) is

$$G = -\frac{\delta\left(t - \tau - \left\|\vec{x} - \vec{\xi}(\tau) - M(t-\tau)\vec{e}_x\right\|\right)}{4\pi\left\|\vec{x} - \vec{\xi}(\tau) - M(t-\tau)\vec{e}_x\right\|}, \tag{6}$$

in which $\vec{e}_x$ is the unit vector in x-direction and $t > \tau$. It follows that the solution of Eq. (3) and hence the solution of Eq. (1) is

$$p = -\int_{-\infty}^{\infty} \frac{\sigma(\tau)\delta\left(t - \tau - \left\|\vec{x} - \vec{\xi}(\tau) - M(t-\tau)\vec{e}_x\right\|\right)}{4\pi\left\|\vec{x} - \vec{\xi}(\tau) - M(t-\tau)\vec{e}_x\right\|} d\tau. \tag{7}$$

Now introduce the emission time $\tau_e(t)$, which is the solution of

$$t - \tau_e = \left\|\vec{x} - \vec{\xi}(\tau_e) - M(t-\tau_e)\vec{e}_x\right\|. \tag{8}$$

As long as the motion is subsonic, this solution is unique. Using Eq. (8) and the identity[10]

$$\int_{-\infty}^{\infty} f(\tau)\delta\big(g(\tau)\big)d\tau = \sum \frac{f(\tau_0)}{g'(\tau_0)}, \text{ where } g(\tau_0)=0\,, \quad (9)$$

Eq. (7) can be worked out as

$$p(\vec{x},t) = \frac{\sigma(\tau_e)}{4\pi\left\{t-\tau_e+Q\left(\vec{x},\vec{\xi}(\tau_e),t,\tau_e\right)\right\}}\,, \quad (10)$$

in which Q is the inner product

$$Q = \left[-\vec{\xi}'(\tau_e)+M\vec{e}_x\right]\cdot\left[\vec{x}-\vec{\xi}(\tau_e)-M(t-\tau_e)\vec{e}_x\right]. \quad (11)$$

It follows that the transfer function T from moving source in $\vec{\xi}(t)$ to receiver in $\vec{x}$ is given by

$$T\left(\vec{x},\vec{\xi}(\tau_e),t,\tau_e\right) = \frac{1}{4\pi\left\{t-\tau_e+Q\left(\vec{x},\vec{\xi}(\tau_e),t,\tau_e\right)\right\}}\,, \quad (12)$$

where the relation between t and τ_e is given by Eq. (8).

Effect of wind tunnel shear layer

The transfer function *T*, derived in the foregoing, is only valid for uniform flow. In other words, the receiver position $\vec{x}$ has to be inside the flow. For out-of-flow array measurements in an open jet wind tunnel, the effect of transmission through the shear layer has to be incorporated in the transfer function.

A simple, but effective way of incorporating the influence of the shear layer in the transfer function is to replace in Eqs. (8) and (11) the uniform flow Mach number by the average mach number between source and receiver.

For instance, if the wind tunnel shear layer is defined by $z = z_s$, then the corrected Mach number is given by

$$M_{\text{cor}} = M\,\frac{\zeta(\tau_e)-z_s}{\zeta(\tau_e)-z}\,, \quad (13)$$

where z and $\zeta(\tau_e)$ are the *z*-coordinates of $\vec{x}$ and $\vec{\xi}(\tau_e)$, respectively.

This shear layer correction, which may seem a little crude, has been extensively compared with two more sophisticated methods: the Amiet correction[11] for an infinitely thin shear layer and ray acoustics[12] incorporating the finite thickness of the shear layer.

This comparison was done through microphone array simulations with a non-moving monopole source. It revealed that the differences in array output between the three methods were negligible, as long as the Mach number is moderate (say $M \le 0.25$) and the angles between the shear layer and the acoustic rays are not too small (say $\ge 45°$).

Reconstruction of source signal

Suppose $\chi_n(t)$, $n = 1,...,N$ are time signals recorded by N microphones at positions $\vec{x}_n$. If a monopole source, with time-dependent position $\vec{\xi}(t)$, is present, then we can write for the microphone signals

$$\chi_n(t) = T\left(\vec{x}_n,\vec{\xi}(\tau_e),t,\tau_e\right)\sigma(\tau_e)+\varepsilon_n(t)\,, \quad (14)$$

where $\varepsilon_n(t)$ is noise and/or contributions from other sources.

In order to reconstruct the source signal $\sigma(\tau)$ from the microphone signals $\chi_n(t)$, we take in Eq. (14) a fixed emission time τ_e, independent of microphone number. Then the receiver time *t* depends on *n* and it is better to write Eq. (14) as

$$\chi_n(t_n) = T\left(\vec{x}_n,\vec{\xi}(\tau_e),t_n,\tau_e\right)\sigma(\tau_e)+\varepsilon_n(t_n)\,, \quad (15)$$

or, briefly,

$$\chi_n(t_n) = T_n(t_n,\tau_e)\sigma(\tau_e)+\varepsilon_n(t_n)\,. \quad (16)$$

The microphone-dependent receiver times t_n follow from Eq. (8):

$$t_n-\tau_e = \left\|\vec{x}_n - M(t_n-\tau_e)\vec{e}_x - \vec{\xi}(\tau_e)\right\|, \quad (17)$$

of which the solution is:

$$t_n = \tau_e - \frac{M\left(\vec{x}_n-\vec{\xi}(\tau_e)\right)\cdot\vec{e}_x}{1-M^2} + \frac{\sqrt{M^2\left\{\left(\vec{x}_n-\vec{\xi}(\tau_e)\right)\cdot\vec{e}_x\right\}^2+\left(1-M^2\right)\left\|\vec{x}_n-\vec{\xi}(\tau_e)\right\|^2}}{1-M^2}. \quad (18)$$

A reconstructed source signal $\tilde{\sigma}(\tau_e)$ can be found with the delay-and-sum procedure[13]:

$$\tilde{\sigma}(\tau_e) = \frac{1}{N}\sum_{n=1}^{N}\tilde{\sigma}_n(\tau_e), \tag{19}$$

where

$$\tilde{\sigma}_n(\tau_e) = \chi_n(t_n)/T_n(t_n,\tau_e). \tag{20}$$

Reconstruction of power spectrum
A straightforward way to calculate the frequency spectrum of the source signal is to evaluate Eq. (19) for $\tau_e = j\times\Delta t,\ j = 1,...,J$ and then perform a discrete Fourier transform:

$$\Im(\tilde{\sigma}) = \frac{1}{N}\sum_{n=1}^{N}\Im(\tilde{\sigma}_n). \tag{21}$$

For the auto-power spectrum we have

$$\frac{1}{2}\left|\Im(\tilde{\sigma})\right|^2 = \frac{1}{2N^2}\left|\sum_{n=1}^{N}\Im(\tilde{\sigma}_n)\right|^2 = \frac{1}{2N^2}\sum_{n=1}^{N}\sum_{m=1}^{N}\Im(\tilde{\sigma}_n)\Im(\tilde{\sigma}_m)^*, \tag{22}$$

in which the asterisk denotes complex conjugation.

Error estimate
With Eqs. (16), (20) and (22), we can write

$$\frac{1}{2}\left|\Im(\tilde{\sigma})\right|^2 = \frac{1}{2}\left|\Im(\sigma) + \frac{1}{N}\sum_{n=1}^{N}\Im\left(\varepsilon_n/T_n\right)\right|^2. \tag{23}$$

Now assume that $\varepsilon_n(t)$ is stochastic and incoherent from one microphone to the other (e.g. wind noise). Then, after averaging over a sufficient number of time periods, the following expression remains:

$$\frac{1}{2}\left|\Im(\tilde{\sigma})\right|^2 = \frac{1}{2}\left|\Im(\sigma)\right|^2 + \frac{1}{2N^2}\sum_{n=1}^{N}\left|\Im\left(\varepsilon_n/T_n\right)\right|^2. \tag{24}$$

Alternative reconstruction of power spectrum
Consider the following alternative for Eq. (22):

$$\frac{1}{2}\left|\Im(\tilde{\sigma})\right|^2 = \frac{1}{2N(N-1)}\left(\left|\sum_{n=1}^{N}\Im(\tilde{\sigma}_n)\right|^2 - \sum_{n=1}^{N}\left|\Im(\tilde{\sigma}_n)\right|^2\right). \tag{25}$$

Again under the assumption that $\varepsilon_n(t)$ is stochastic and incoherent, and after averaging over many time periods, we simply get

$$\frac{1}{2}\left|\Im(\tilde{\sigma})\right|^2 = \frac{1}{2}\left|\Im(\sigma)\right|^2, \tag{26}$$

in other words, the expected error is zero now.

This alternative method, which is analogous to the well-known method of ignoring the main diagonal of the cross-correlation matrix, looks almost perfect. Indeed, it is very convenient in noisy environments, but the method does have its drawbacks. If errors do exist, for instance if a secondary source exists (giving a coherent contribution to $\varepsilon_n(t)$) or in case of insufficient averaging, then the right-hand side of Eq. (25) may become negative, which is not physical.

Need for oversampling
In the reconstruction of source signal and power spectrum, microphone data are needed at times t_n, given by Eq. (18). Unfortunately, these times do not coincide with the times at which the measurement system samples the data. The best way to proceed is to linearly interpolate the measured data. To avoid the frequency spectrum from being spoiled by side lobes from higher frequencies, the sample frequency should be taken higher than two times the maximum analysis frequency, without raising the low pass filter cut-off frequency. This problem was addressed for instance by Howell et al[7].

III. Applications

Computer program ROSI
Based on the theory described in the previous chapter, the computer program ROSI has been written to locate rotating sources and reconstruct their emitted signals. ROSI assumes point sources with unidirectional directivity (monopoles). However, any other a priori known directivity could be included by converting the right-hand side of Eq. (1) into a multipole expansion. For the estimation of power spectra, ROSI uses the "alternative method" (see previous chapter).

The rotational speed, which may slowly vary, is determined by tacho pulses generated once per revolution. The source may rotate in a uniform flow and the array may be placed out-of-flow (open jet wind tunnel set-up).

Rotating whistles
For validation of ROSI, an experiment in the anechoic chamber of the NLR Small Anechoic Wind Tunnel KAT was set up, consisting of microphone array measurements on rotating sources. The rotating sources were two whistles producing pure tones at

different frequencies. The whistles were mounted at the tips of two tubes connected to an exciter (Fig. 1). The radius of the circle described by the whistles was 0.56 m.

The array used in this experiment consisted of 35 microphones arranged in a sparse 2D set-up[14], the same as used by Oerlemans and Sijtsma[15]. In order to record Doppler-shifted frequencies, the array was positioned at an oblique view angle (Fig. 2).

Both the frequency of the whistles and the rotational speed of the tubes were varied in the experiment. Here, we consider the frequencies 3150 Hz (whistle 1) and 5000 Hz (whistle 2), and 354 RPM for the rotational speed.

First, it was confirmed that ROSI is able to reconstruct the emitted sound when the whistles are non-rotating. This is shown in Fig. 3 and Fig. 4, where the power level of the central microphone in the array is plotted against power spectra reconstructed by ROSI focusing on the respective whistles. At the main frequencies the peak levels of the main frequencies are perfectly recovered. Furthermore, whistle 2 generates some noise around 1600 Hz, which is recovered also. At the second harmonic of whistle 1 (6300 Hz), there is some "underprediction" in level, due to loss of coherence between the microphone signals.

It is noted that the reconstructed level for whistle 1 drops down at the frequency of whistle 2 and vice versa. This is an artefact of the alternative method for power level reconstruction described in the previous chapter.

When the whistles are rotating, Doppler-shift of frequencies occurs. This is illustrated in Fig. 5, where the power spectra are compared for the non-rotating and for the rotating whistles.

It is observed that, at the higher frequencies (base frequency of whistle 2 and 2nd harmonic of whistle 1), the Doppler-shift is more towards lower than towards higher frequencies. This is attributed to the directivity of the whistles. Because of this, less noise is perceived when a whistle moves towards the array than when it moves away.

The ability of ROSI to reconstruct power levels of rotating whistles is shown in Fig. 6 and Fig. 7, where the power level for non-rotating whistles is compared with spectra reconstructed by ROSI in case of rotating whistles. In general, the ROSI results are good. For 5000 Hz (Fig. 7), there is a small reduction in peak frequency due to the before mentioned directivity effects.

Helicopter blades

In the open configuration of the DNW-LLF, measurements were done on a five-bladed helicopter model with 4 m diameter rotor plane, using a 136 microphone acoustic array (see Fig. 8). The array was basically the same 4x4 m^2 array of 100 microphones as used by Dobrzynski et al[16], however, extended at the corners with four diagonal 1.5 m arms to increase the resolution. For practical reasons, the array was not placed directly below the rotor plane.

To test ROSI, array measurements were used of a "hover" configuration without wind and without shaft angle (horizontal rotor plane). In that case, there is no generation of impulsive blade-vortex interaction noise. Typical results are shown here for 852 RPM.

First, the measurements were processed using conventional array software, assuming non-rotating point sources. Typical results (at 2000 Hz, 1/3 octave) are shown in Fig. 9. The absolute levels do not make much sense here, since the point source assumption clearly did not hold.

What we can learn from Fig. 9 is that a circular source region exists at a short distance from the blade tips. Also, the shadow of the body can be recognised. The noise mechanism may be (continuous) interaction of the helicopter blades with tip vortices from neighbouring blades or it could be airfoil self-noise. The sound sources are located somewhat inside the tip radius. This does not rule out the possibility of continuous blade-vortex interaction, as the vortices are contracted in the downwash. Similar source circles, at the same location, were observed at other frequencies.

Next, ROSI was applied. The same grid of focal points was used as in Fig. 9, but now rotating with the rotor. The results are plotted in Fig. 10. Instead of a fairly uniform distribution of noise sources, we now observe clear peaks at the blade positions. In other words, the noise sources are fixed to the blades. Since the sources are now concentrated on five positions, the peak levels in Fig. 10 are higher than in Fig. 9. Reconstruction of the narrow-band power spectra of the source signals, emitted from these peak locations, reveal that these sources have a broadband character (Fig. 11).

Wind turbine blades

Measurements were done in the open jet of the DNW-LLF on a 4.5 m diameter two-bladed wind turbine

rotor model, with the same acoustic array of 136 microphones as used for the helicopter measurements (see Fig. 12). The purpose of the experiments was to determine aerodynamic noise levels of different blades for various conditions[9]. For all results shown here, the RPM was 424, the tunnel speed was 14 m/s, and the yaw angle was 0°.

The acoustic source distribution in the rotor plane, as obtained by conventional array software (non-rotating sources), is given in Fig. 13a, where the black circle indicates the trajectory of the blade tips. Apparently, a broadband aerodynamic source is present at a radius of about 2 m. The noise from this source is concentrated in the right-hand sides of the plots. This is not because the noise sources are circumferentially asymmetric, but because of different array perception. In the right-hand sides of the plots, the blades move in the direction of the array. In that case, the array perceives more noise, due to source directivity and convective amplification. The source at the centre of the plot is due to mechanical noise from the rotor hub. At 8 kHz a second aerodynamic source is observed, at 0.5 m from the hub.

Fig. 13b shows the corresponding ROSI plots for the same measurement. The black line indicates the contour of the blade (trailing edge on upper side). These plots give the de-Dopplerised acoustic source levels, summed for both blades. The broadband aerodynamic source can clearly be located at the trailing edge, while the 8 kHz source at a radius of 0.5 m turns out to be located at the leading edge of the blade. This extraneous source, which was only present at one of the two rotor blades, was found at the junction of two different blade shapes (see Fig. 14).

The signal/noise ratio in the ROSI plots is much higher than in the conventional plots, although for the ROSI plots only 2 seconds of measurement time were used (compared to 60 seconds for the conventional plots). This is because the signal level increases by about 6 dB, while the noise level stays the same. This improvement in signal/noise ratio is even better illustrated in Fig. 15, which compares conventional and ROSI source plots for a rotor with relatively silent blades. Whereas in the conventional plot no aerodynamic sources can be detected due to the low sound level, the ROSI plot clearly shows the trailing edge noise source on the blades.

To further illustrate the capabilities of the method, Fig. 16 shows the effect of trailing edge treatment ("serrations"). For the same rotor and identical conditions, a clear reduction is observed in trailing edge noise levels at the location of the serrations.

IV. Conclusions

A theory was developed to locate moving sources and to reconstruct their emitted signals by microphone array measurements. Application is possible to any subsonic motion, embedded in a uniform flow. Out-of-flow measurements, as in an open jet wind tunnel, are feasible too.

For the reconstruction of source power spectra, a method yielding high signal/noise ratios was proposed, analogously to the well-known method of ignoring the main diagonal of the cross-correlation matrix.

The theory was implemented for rotating sources. A computer program was written and applied to rotating whistles, helicopter blades in hover and wind turbine blades in uniform flow. Rotating sources, both tonal and broadband, were well identified.

Acknowledgement

This work has been carried out partly in the framework of the JOULE project "Design and Testing of Acoustically Optimized Airfoils for Wind Turbines" (DATA) under contracts awarded by the European Commission and the Netherlands Agency for Energy and Environment, NOVEM BV, and partly within the "Update II" project of the German Dutch Wind Tunnel DNW: "Development of a Microphone Array System". The authors are grateful to ATIC for their permission to use the helicopter measurements.

References

[1] Holthusen, H., and Smit, H., "A new data acquisition system for microphone array measurements in wind tunnels", AIAA paper 2001-2169, 2001.

[2] Takano, Y., Horihata, K., Kaneko, R., Matsui, Y., and Fujita, H., "Analysis of sound source characteristics of Shinkansen cars by means of x-shaped microphone array", Internoise 96, Liverpool, 1996.

[3] Barsikow, B., "Experiences with various configurations of microphone arrays used to locate sound sources on railway trains operated by the DB AG", JSV 193(1), pp. 283-293, 1996.

[4] Michel, U., Barsikow, B., Helbig, J., Hellmig, M., and Schüttpelz, M., "Flyover noise measurements on landing aircraft with a microphone array", AIAA Paper 98-2336, 1998.

[5] Piet, J.-F., and Elias, G., "Localization of acoustic

source from a landing aircraft with a microphone array", AIAA Paper 99-1811, 1999.

[6] Barsikow, B., and King III, W.F., "On removing the Doppler frequency shift from array measurements of railway noise", JSV 120(1), pp. 190-196, 1988.

[7] Howell, G.P., Bradley, A.J., McCormick, M.A., and Brown, J.D., "De-Dopplerization and acoustic imaging of aircraft fly-over noise measurements", JSV 105(1), pp. 151-167, 1986.

[8] Howe, M.S., *Acoustics of Fluid-Structure Interactions*, Cambridge University Press, 1998.

[9] Oerlemans, S., Schepers, G., Guidati, G., and Wagner, S., "Experimental demonstration of wind turbine noise reduction through optimized airfoil shape and trailing-edge serrations", to be presented at the European Wind Energy Conference and Exhibition, Copenhagen, Denmark, 2-6 July 2001

[10] Dowling, A.P., and Ffowcs Williams, J.E., *Sound and Sources of Sound*, Wiley, 1983.

[11] Amiet, R.K., "Refraction of sound by a shear layer", JSV 8(2), pp. 467-482, 1978.

[12] Schulten, J.B.H.M., "Computation of Aircraft Noise Propagation through the Atmospheric Boundary Layer", Proc. 5th Int. Congress on Sound and Vibration, Adelaide, Australia, 1997.

[13] Johnson, D.H., and Dudgeon, D.E., Array Signal Processing, Prentice Hall, 1993.

[14] Sijtsma, P., "Optimum arrangements in a planar microphone array", presented at the First CEAS-ASC Workshop: Wind Tunnel Testing in Aeroacoustics, DNW, 5/6 November 1997.

[15] Oerlemans, S., and Sijtsma, P., "Effects of wind tunnel side-plates on airframe noise measurements with phased arrays", AIAA Paper 2000-1938, 2000.

[16] Dobrzynski, W., Chow, L.C., Guion, P., and Shiells, D., "A European study on landing gear airframe noise sources", AIAA Paper 2000-1971, 2000.

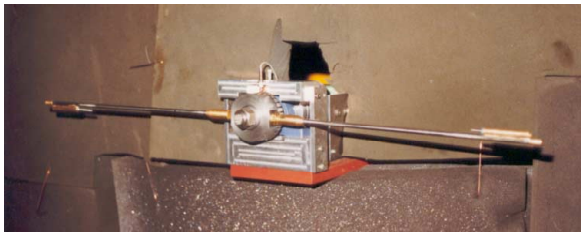

Fig. 1 Rotating whistles

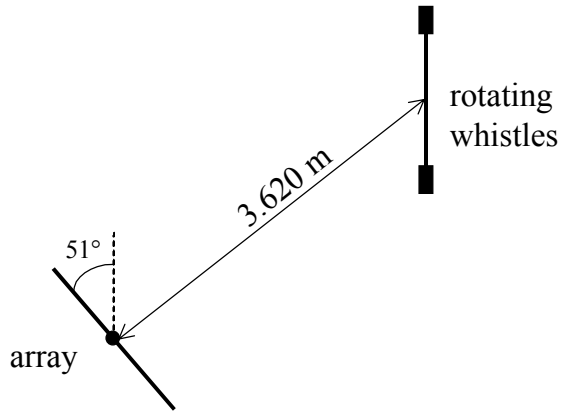

Fig. 2 Sketch of set-up with rotating whistles and microphone array

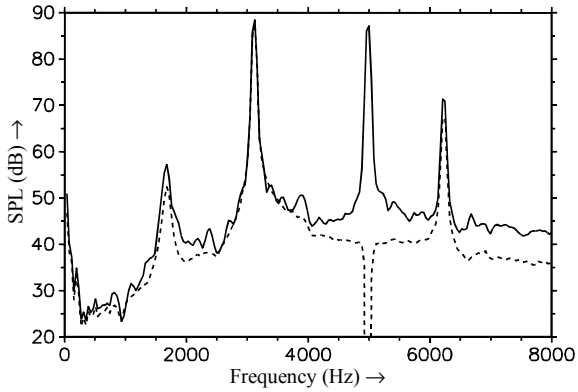

Fig. 3 Power spectra at central array microphone: — non-rotating whistles; --- ROSI reconstruction, non-rotating case, focusing on whistle 1

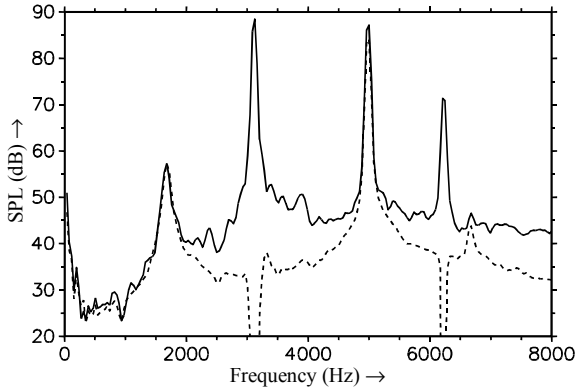

Fig. 4 Power spectra at central array microphone: — non-rotating whistles; --- ROSI reconstruction, non-rotating case, focusing on whistle 2

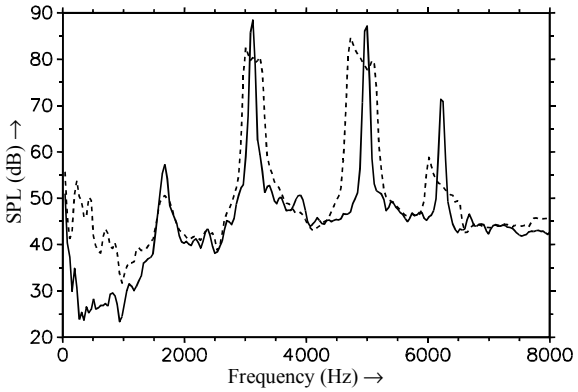

Fig. 5 Power spectra at central array microphone: — non-rotating whistles; --- rotating whistles

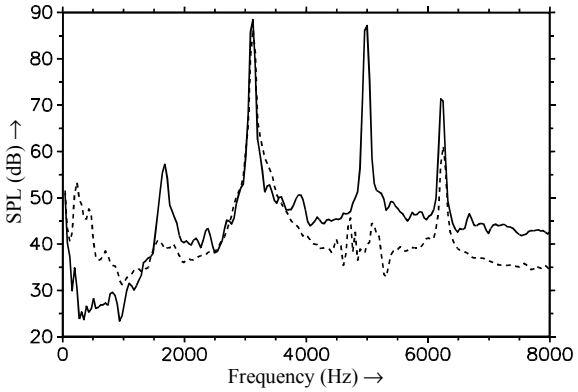

Fig. 6 Power spectra at central array microphone: — non-rotating whistles; --- ROSI reconstruction, rotating case, focusing on whistle 1

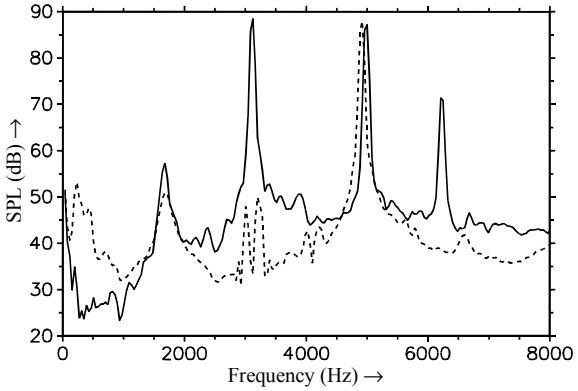

Fig. 7 Power spectra at central array microphone: — non-rotating whistles; --- ROSI reconstruction, rotating case, focusing on whistle 2

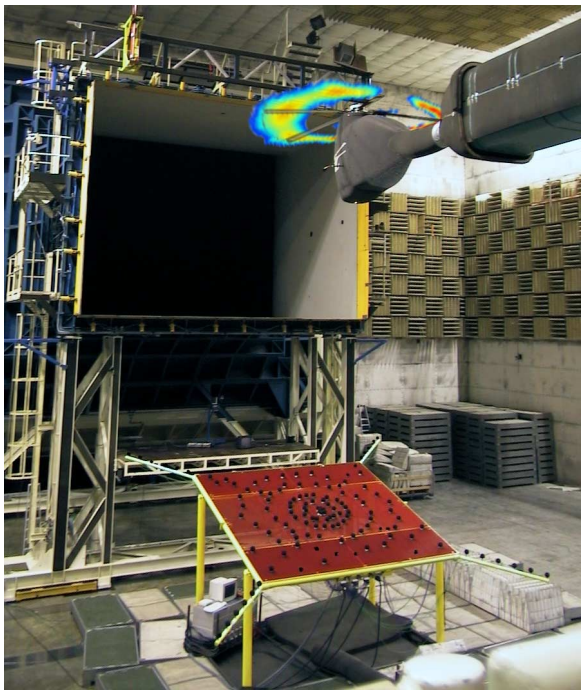

Fig. 8 Test set-up in DNW-LLF, with model scale helicopter and acoustic array; with projection of typical acoustic source distribution (conventional array software) in the rotor plane

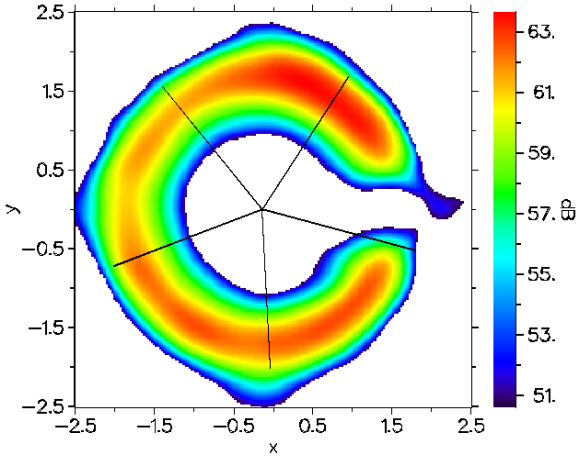

Fig. 9 Conventional acoustic source plot of helicopter in hover, assuming non-rotating sources, 2000 Hz

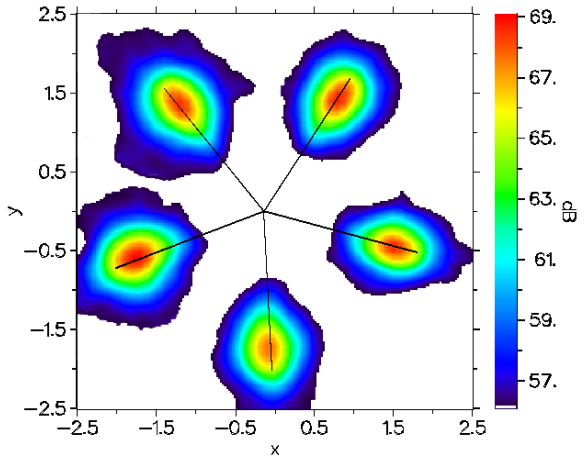

Fig. 10 ROSI source plot of helicopter in hover, 2000 Hz

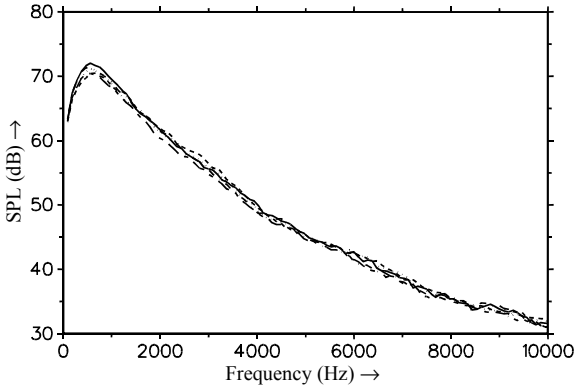

Fig. 11 ROSI narrow-band results, focusing on peak locations in Fig. 10

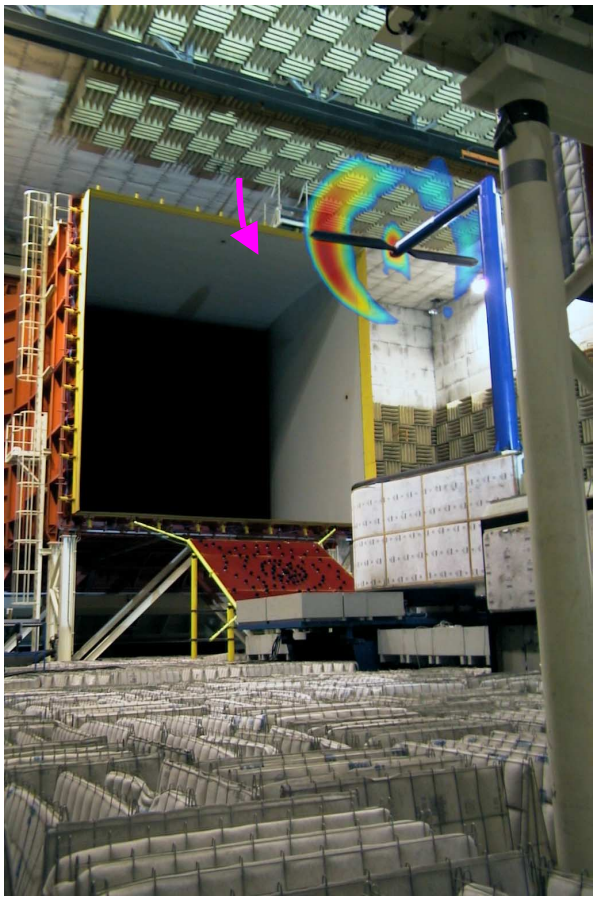

Fig. 12 Test set-up in DNW-LLF, with model scale wind turbine and out-of-flow acoustic array; with projection of typical acoustic source distribution (conventional array software) in the rotor plane, 3150 Hz

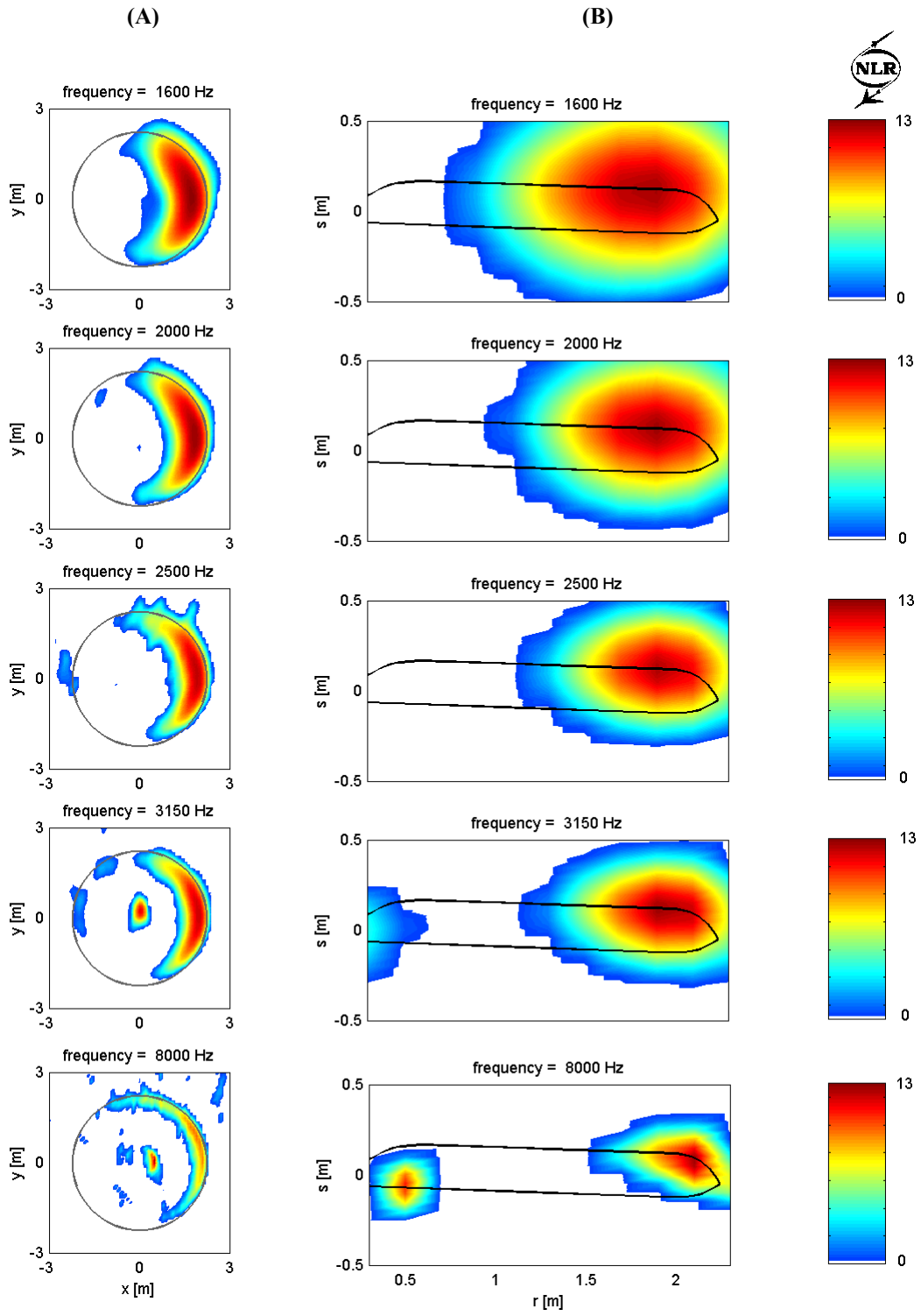

Fig. 13 (a) Conventional acoustic source plots of rotor plane (b) ROSI source plots of rotating blades; all levels are normalised with respect to the maximum level in the plot; the dynamic range is 13 dB

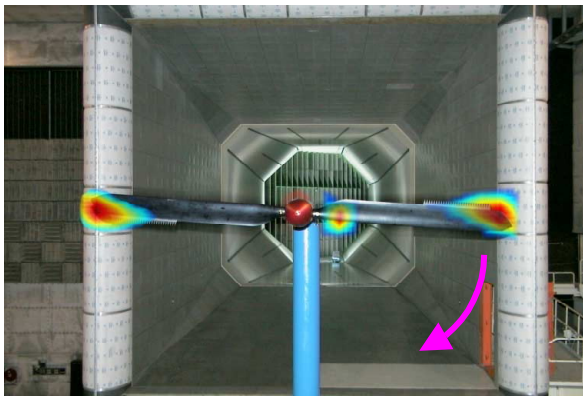

Fig. 14 Picture of wind turbine rotor; the source distribution on the rotating blades (ROSI) is projected onto the picture, 8000 Hz

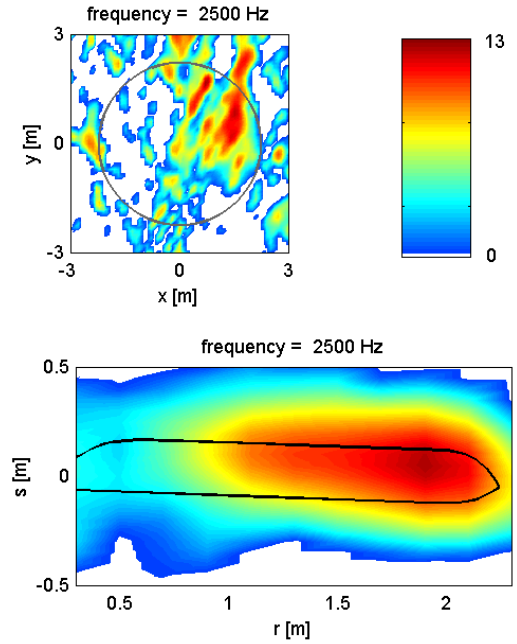

Fig. 15 Comparison of conventional and ROSI source plot for measurement with low sound level, illustrating the improvement in signal/noise ratio

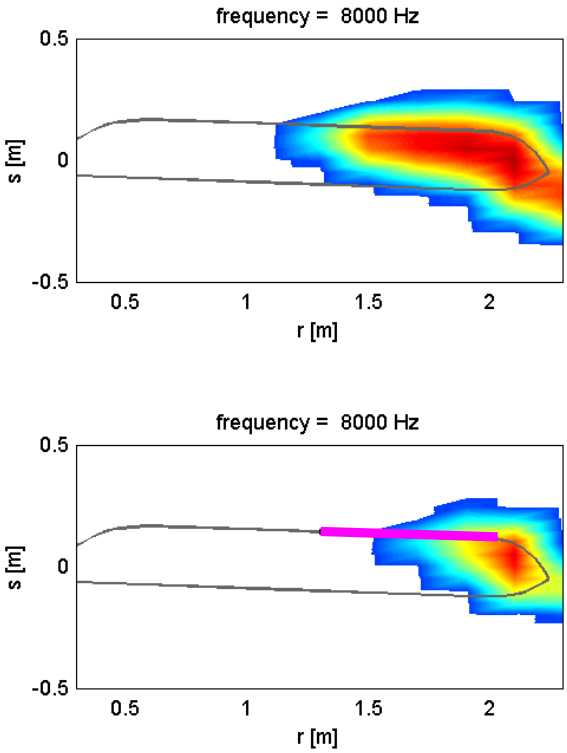

Fig. 16 Effect of trailing edge serrations on radiated trailing edge noise, for the same rotor and identical flow conditions; the position of the serrations is indicated with the violet line (lower plot)